Nanoscale Advances

ROYAL SOCIETY OF CHEMISTRY

PAPER

View Article Online
View Journal | View Issue

Cite this: *Nanoscale Adv.*, 2020, **2**, 4070

pH-regulated thermo-driven nanofluidics for nanoconfined mass transport and energy conversion†

Xiaolu Zhao,‡[abc] Long Li,‡[b] Wenyuan Xie,[b] Yongchao Qian,[ac] Weipeng Chen,[ac] Bo Niu,[ac] Jianjun Chen,[ac] Xiang-yu Kong,[a] Lei Jiang[ac] and Liping Wen *[ac]

Received 27th May 2020
Accepted 16th July 2020

DOI: 10.1039/d0na00429d

rsc.li/nanoscale-advances

Bioinspired nanochannels whose functions are similar to those of the biological prototypes attract increasing attention due to their potential applications in signal transmission, mass transport, energy conversion, *etc.* Up to now, however, it is still a challenge to extract low-grade waste heat from the ambient environment in an aqueous solution. Herein, a thermo-driven nanofluidic system was developed to extract low-grade waste heat efficiently based on directed ionic transport at a micro-/nanoscale. A steady streaming current increases linearly with the temperature gradient, achieving as high as 14 nA at a temperature gradient of 47.5 °C (δT = 47.5 °C) through a 0.5 cm^2 porous membrane (10^6 cm^{-2}). And an unexpected theoretical power of 25.48 pW using a single nanochannel at a temperature difference of 40 °C has been achieved. This bioinspired multifunctional system broadens thermal energy recovery and will accelerate the evolution of nanoconfined mass transport for practical applications.

1. Introduction

The past decade has witnessed an explosive growth of highly efficient energy conversion systems independent of fossil fuels, which is becoming extremely urgent regarding the greenhouse effect, environmental issues, and energy crisis.[1] More recently, quantities of novel energy conversion systems have been put forward,[2–4] for example, salinity gradient energy conversion,[5] solar cells,[6] water energy harvesting,[7] wind energy conversion,[8] *etc.* In particular, a generator relying on nanochannels is capable of sustaining a stable electric power output driven by low-grade heat, which is widely distributed and abundant.[9] The advantage of easily scaling down to a small size makes it unique to recycle waste heat and implement in microelectronics and portable electronic devices. Such an energy conversion device, if it could be fabricated, would be promising and provide more opportunities to the energy sector.[10]

In terms of the thermodynamics of the underlying process, the exploration of electrokinetic phenomenon at the nanoscale and the promising potential for energy conversion have a long history yet slow development.[10,11] In general, when a liquid phase with electric neutrality is confined to a flow inside a nanochannel, the charge distribution in the electrical double layer (EDL) that is governed by surface attributes will screen co-ions and thus the migration of surplus ions results in a streaming current or voltage difference between the ends of the nanochannel. Some efforts have been made to optimize the geometry and surface chemistry of nanofluidic channels to manipulate the molecular or ion transport behaviours.[12–15] Due to the emersion of complex fluid behaviour introduced by various molecular forces, the poor efficiency limited the utilization of waste heat in dilute electrolytes.[8,9] The underlying mechanism of mechanical or electrical energy recovered from waste heat in confined structures has been extensively studied.[16–18] Li *et al.* investigated the mechanisms of fluid transport driven by temperature gradients in nanochannels through molecular dynamics simulations and found that fluid-wall binding energy played critical roles in the flow direction.[19] Dietzel *et al.* found that the thermoelectric voltage of dilute electrolytes in a confined geometry was solely proportional to the zeta potential or surface charge density of the channel.[20] Although such investigations have confirmed that a streaming current or voltage could be generated by a temperature gradient in a charged nanochannel, there are still many practical issues that need to be addressed before it becomes a good alternative to conventional energy. In particular, a high performance is critical for the commercialization of low-grade heat conversion. Recently, a hydrophobic nanoporous membrane was used to harvest low grade heat using thermo-osmotic vapour, which required an external power supply and was energy-consuming.[21] An external power-free thermoelectric conversion system using

[a]*CAS Key Laboratory of Bio-inspired Materials and Interfacial Science, Technical Institute of Physics and Chemistry, Chinese Academy of Sciences, Beijing 100190, PR China. E-mail: wen@mail.ipc.ac.cn*

[b]*Qian Xuesen Laboratory of Space Technology, Beijing 100049, PR China*

[c]*University of Chinese Academy of Sciences, Beijing 100049, PR China*

† Electronic supplementary information (ESI) available. See DOI: 10.1039/d0na00429d

‡ These authors contributed equally to this work.

a directed ionic flow through a biomimetic smart nanochannel was also introduced, however, the thermopower was unattractive.[22] A silica nanochannel/PET hybrid membrane was fabricated to quantitatively describe thermally sensitive permselective ion transport and demonstrated a high system efficiency, but a scalable implementation of inorganic membrane often brought reliable issues.[23] Nevertheless, the development of new materials is necessary to bridge the state-of-the-art technology and further applications on low-grade heat energy conversion.

Thermo-driven nanofluidics are not artificial, and are ubiquitous in organisms where ion transport is regulated by ion channels in response to complex external stimuli, which lays the foundation for the life sciences.[15] Unfortunately, it is difficult for biological prototypes to implement various essential physiological functions *in vitro* due to fragility and inactivation. Inspired by these ion channels, bioinspired solid-state nanochannels have been put forward in past decades to mimic delicate functions such as ion gating, ion selection and ion rectification.[24,25] Transient receptor potential channels (TRPs) identified in corneal tissue layers and cells (skin organ) are Ca^{2+} permeable channels, most of which serve as thermosensitive molecular sensors (thermo-TRPs).[26–28] Modulation of the intracellular Ca^{2+} influx (such as transient increases) as a consequence of channel activation by environmental temperature change is essential for tissues to offset declines in physiological functions.[29] The extremely rapid transmittance of specific ions guarantees a complicated and instant stress reaction.[30] Learning from thermo-TRP, bioinspired solid-state nanochannels were expected to harvest low-grade waste heat efficiently.

In this work, we develop a heterogeneous nanoporous membrane, one side which is polydopamine (PDOPA) and the other side is polyimide (PI). The dopamine grafted in the nanochannel bears a positive or negative charge depending on pH conditions. It was found that the charge species and its asymmetric distribution play critical roles in mass transfer and energy conversion. The theoretical maximal power achieves 25.48 pW in a single nanochannel under a temperature difference of 40 °C. A large augmentation of output power can be realized theoretically by scale-up fabrication of the porous membrane. A steady streaming current increases linearly with the temperature gradient, achieving as high as 14 nA at 47.5 °C through a 0.5 cm^2 porous membrane (10^6 cm^{-2}), and even though it exerts multiple deliberate disturbances at various temperatures and pressures, it approaches 3 nA at a temperature gradient of 7 °C under an adverse pressure gradient of 500 Pa. The nanodevice opens opportunities for a new avenue in nanoconfined mass transport and thermal energy recovery towards real-world applications.

2. Results and discussion

Characterization of PDOPA-modified PI membrane

The PI membrane (12 μm) was firstly prepared by an ion track etching technique and then it was chemically modified by DOPA (Section S1†). The diameter of the base side in a conical nanochannel was about 750 nm while the tip diameter was about 180 nm (Section S2†). The conical nanochannel was fabricated with the PI membrane, which was asymmetrically modified by the self-polymerization of dopamine (Fig. S3A†). The transmittance of the modified membrane was weaker than that of the naked membrane in ultraviolet-visible spectroscopy (Fig. S3B†). The contact angle was tested using a 2 μL waterdrop as a prerequisite that the membranes were immersed into solutions with different pH for 2 hours. Compared with the bare PI membrane, the contact angle (θ) of the modified PI membrane changed from $53.56 \pm 1.47°$ to $78.94 \pm 2.19°$ while the charged planar film became more hydrophilic due to a strong polarization (Fig. S3C†). The wetting behaviour of the nanoconfined region was totally different between prior and post modification, which plays a pivotal role in fluid dynamics.[31] A strong liquid–wall interaction leads to considerable fluid density variation in the hydrophilic nanochannels, influencing thermo-driven flow.[32–34]

pH-induced amphoteric response

Inasmuch as the chemical composition and polymerization mechanism are ambiguous, the enthusiasm for further analysis and application has not extinguished in consideration of abundant functional groups and versatile adhesion. The self-polymerization feature of DOPA has been studied intensively by numerous groups since it was first applied to modify various surfaces by Messersmith *et al.*[35] Due to the effect of DOPA on the tip side, the ion selectivity of the modified membrane increased than before, explicating the length of the critical region at which the electrical double layer functions as "an ion filter" (Section S5, Fig. S4†). The contemplated design of polydopamine renders simultaneous amino and hydroxyl groups, which bestows them with the competence of negative or positive charge (Fig. 1A). When the *I–V* curves were measured at different pH conditions following the sequence of 6.5, 11, 3, the rectification varies from anion selectivity to cation selectivity (Fig. 1B), corresponding to a non-ohmic law that in turn affirms the presence of an amphoteric surface charge. Ion rectification has been intensively studied in different kinds of conventional nanoscale pores where the thickness of the EDL is comparable to the diameter of the small openings.[36–38] The thickness of the EDL is absolutely less than 3 nm for 0.1 mol L^{-1} KCl. However, the diameter of the tip side reaches 180 nm so that the aperture is far more than the thickness of the EDL. Such an anomalous rectification phenomenon is accounted for by the high charge density of the polymer-based interface and high ion mobility of H^+ or OH^-.[39,40] The measured transmembrane ionic conductance deviated from bulk values (dotted line) when the KCl concentration was less than 0.1 mol L^{-1} (Fig. 1C). The thickness of the EDL is inversely proportional to the bulk concentration (Section S6†). That charge-governed ionic transport emerged at such a high bulk concentration is accounted for by a high charge density inside the channel of the heterogeneous membrane. Furthermore, the zeta potential of the modified planar membrane was measured to support the surface charge changing from positive to negative (Fig. 1D).

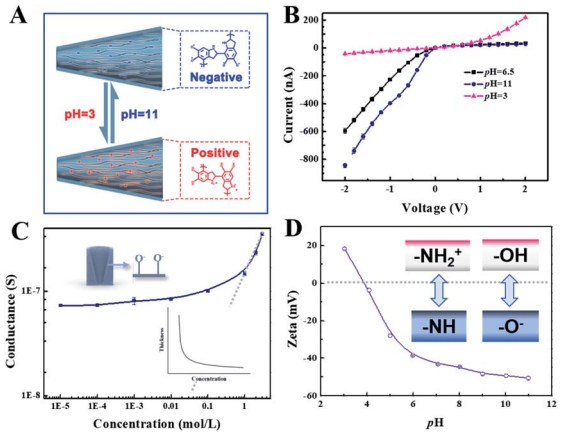

Fig. 1 The amphoteric response of a modified nanochannel. (A) Schematic illustration of the polydopamine with the competence of a negative or positive charge at different pH following the sequence of 6.5, 11, 3. (B) *I*–*V* curves of the modified PI membrane under a 0.1 mol L^{-1} KCl solution at different pH conditions scanning from −2 to 2 V 10 times. The anode was set near the base side. (C) The transmembrane conductance at different concentrations. The inset is the schematic function diagram of the thickness of the EDL *versus* bulk concentration (Section S5†). (D) Zeta potential of the modified planar membrane. It was measured in the presence of 1 mmol L^{-1} KCl which pH adjusted before the measurement.

pH-regulated thermo-driven flow

The experimental setup is shown on Section S7 in detail.† The capability of power generation was examined with a customized device (Fig. S5†). In all cases, the anode was set near the base side and the device was aligned to the horizontal position in advance (Fig. S6†). The streaming current ensued immediately the temperature difference emerged. For pH = 3, the inner surface was governed by a positive charge and possessed anion selectivity. When the base was set near the hot side, the observed streaming current was recorded up to −1.5 nA at 59.51 °C (δT) (Fig. 2A). Conversely, when the base was near the cold side, the recorded streaming current struck 2.3 nA at 61.65 °C (δT) (Fig. 2B). The different current absolute values represent that a preferential direction of anion flow was observed as a result of the asymmetric distribution of functional groups in a conical nanochannel. When pH = 11, the inner surface was governed by a negative charge allowing the cation to transport freely. When the base was placed close to the hot side, a negative current was obtained, approximately −3 nA at δT = 50 °C (Fig. 2C). Although the negative current was similar to that in the acidic condition, the cation flowed in the nanochannel rather than the anion. In this case, we analysed the flow direction change due to the surface charge changing. By replacing in the opposite direction, a positive current of approximately 3 nA at δT = 55 °C was obtained (Fig. 2D).

As observed, the current was variable at identical pH conditions on tuning the direction of the conical nanochannel facing the hot side (tip-hot or base-hot), which was accounted for by the asymmetric geometry of nanochannel. According to the racket mode,[41] the electrostatic interaction, which originates from the ions passing through the nanopore and the pore walls, facilitates the cations to flow from the tip to the base side in alkaline conditions and the anions to flow from the tip to the base side in acidic conditions. It was speculated when thermal energy was used as a driving force, the effect of surface charge would be similar. For a negatively charged nanochannel, the positive ions are transported preferentially from the tip to the base side. However, for a positively charged nanochannel, the opposite ions are transported preferentially (Fig. S7†). Thus, as the membrane was placed in the prior direction of the electrostatic interaction and the direction of the temperature field identical, the absolute value of the streaming current is bigger. Although the ion distributions of amino groups and hydroxyl groups were similar in the same nanochannel for different pH conditions, the charge density of hydroxyl groups excelled that of the amino groups because of a greater preponderance of the number of and stronger electronegativity of oxygen. Thus, the streaming current generated at pH = 11 was superior to that at pH = 3.

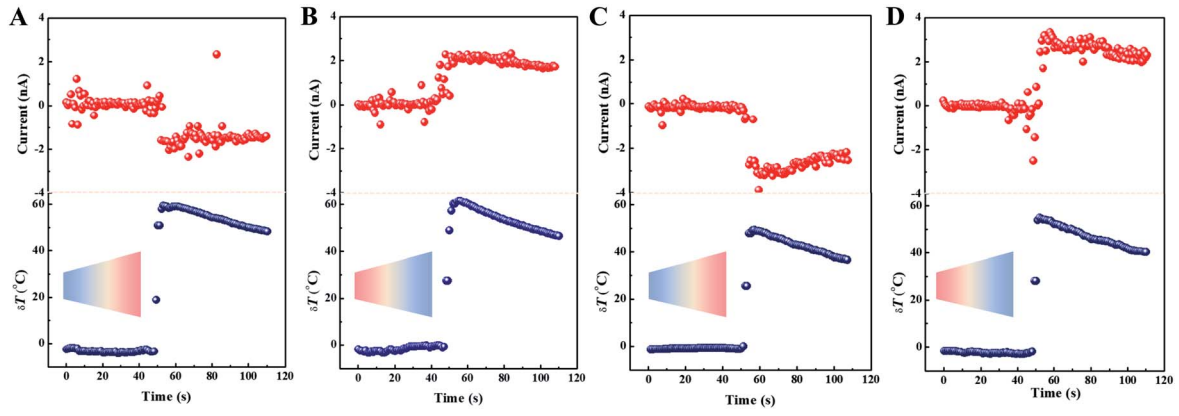

Fig. 2 Streaming current obtained by low-grade thermal energy. Streaming current at different pH conditions (the inset is the setup): at pH = 3, (A) the base side was set toward the hot source. (B) The opposite direction. At pH = 11, (C) the base side was set toward the hot source. (D) The opposite direction. The majority of flowing ions was Cl^- when the surface was governed by a positive charge, and the majority of flow ions was K^+ when the surface was governed by a positive charge.

The mechanism was investigated from the aspect of thermoosmosis. As a premise, the effects of electrode and ion diffusion were ignored. The membrane possesses an opposite ion selectivity at alkaline or acid conditions. The majority of flowing ions was Cl^- when the surface was governed by a positive charge, and the majority of the flowing ions was K^+ when the surface was governed by a positive charge. Assuming the fluid direction is identical at different pH conditions, the current direction should be the opposite. However, the corresponding current direction was the same (Fig. 2A–D). This was accounted for by the flowing direction changing reversely. The fluid density near the wall at a low temperature area was higher than that at the high temperature area at pH = 11 due to a liquid–wall interaction, pushing the fluid to migrate from the high density area. Hence, the fluid favours moving from a low temperature to a high temperature.[42] But the flow direction changed reversely when the pH conditions became alkaline, which mechanism was quantitatively elucidated by numerical simulations based on solving the Poisson–Nernst–Planck (PNP) equations, Naiver–Stokes (NS) equations as well as energy equations.[43] In this work, we simplified the system rationally as a conical channel with two cell reservoirs, which is common in previous literature.[36,44] The detailed parameters are listed in Section S10.† For convenience, the base side was grounded uniformly (Fig. S9AII–DII†). In the simulation, the thermal slip coefficient is dependent on the surface charge density, resulting in a change of liquid velocity at the hydrophilic interface of the pore wall (Section S11†).[20,45] The liquid exhibited a differentiated flow under the dual modulation of a temperature gradient and surface charge. As expected, the fluid flows from cold to hot sources when the inner surface is governed by a negative charge, while the reverse phenomenon occur when changing the surface charge from negative to positive (Fig. S9AIII–DIII†). The voltage generated by liquid flow was affected by the differential flow directions and ion species (Fig. S10†). The directed flow of specific ions resulted in the accumulation and dissipation of ions on two sides of the nanochannel, and thus the voltage difference generated from the hot to the cold source when pH = 11 due to the flow of K^+ from the cold to the hot source and when pH = 3 due to the flow of Cl^- from the hot to the cold source (Fig. S9AIV–DIV†). In addition, it is worth mentioning that highly charged functional groups are beneficial for the formation of EDL, which facilities the Seebeck coefficient in nonequilibrium thermal diffusion-osmosis process, presumably.[46] The generated thermoelectric voltage greatly outperforms that of its bulk counterpart, where the ion mobilities of the counter ion pair (K^+ and Cl^-) were identical or a little different due to the ultrahigh selectivity realized in a nanoconfined geometry.[9] The nanochannel with an asymmetric charge distribution possessed an excellent ion selectivity, which provide a benchmark for the streaming current generation. Further, the pH condition plays a critical role in ion transport.

Thermal energy conversion

To evaluate the capability of the thermoelectricity conversion, we measured the open-circuit voltage (V_{oc}) and short-circuit current (I_{sc}) under an external electric bias from −50 mV to 50 mV (Fig. 3A and B). The electrolyte was 0.1 mol L^{-1} with a normal pH (6.5). The V_{oc} and I_{sc} increased with temperature gradient no matter which side the base direction was placed near (Fig. 3C and D), because the thickness of the EDL is affected by temperature (Section S5†). Apart for V_{oc} and I_{sc}, the conversion capability was expressed by the theoretical maximal outpower (P_{max}), which was obtained by area integral of the *I–V* curves within the coordinate axes. P_{max} had a nonlinearly positive correlation with δT (Fig. 3E). When δT was equal to 40 °C, P_{max} in the forward direction was 15.9 pW (1.86 nA, 17.1 mV) while P_{max} in the reverse direction was only 5.02 pW (1.14 nA, 8.79 mV). Furthermore, the *I–V* curves were measured for the forward direction in a strongly alkaline situation where the electrolyte was 0.1 mol L^{-1} KCl with pH = 11 (Fig. S11†). It was noted that the *I–V* curves were arcuate because of strong rectification even though under small electric bias. As a result of the sharp enhancement of charge density, P_{max} had an enthralling behaviour of 25.48 pW (3.05 nA, 17.1 mV) when the base side was toward the hot source. Similarly, P_{max} decreased to 13.6 pW (1.39 nA, 10.4 mV) when changing the direction of the membrane (Fig. S12†). We compared some recent papers, including an aqueous salty solution and a gel system with a redox pair. Our results excelled those of the aqueous salty solution and rivalled those of other matrices (Fig. S13†).

Beside thermoelectrical estimation, this simple system was developed into a practically applicable thermoelectric conversion nanodevice. It has been mentioned in the preceding part of the text that a streaming current can be generated under a temperature gradient, possessing a designative direction and specific ion. We assumed three situations to exhibit the stability and sensitivity of nanodevices using 0.1 mol L^{-1} KCl solution. The hot electrolyte was stepwise dropped into the system with the volume of 1 mL each time, which was beneficial for enhancing temperature difference. (1) The system was set at room temperature (20 °C) at the first stage, and then the hot electrolytes were fed into the base side continuously at regular

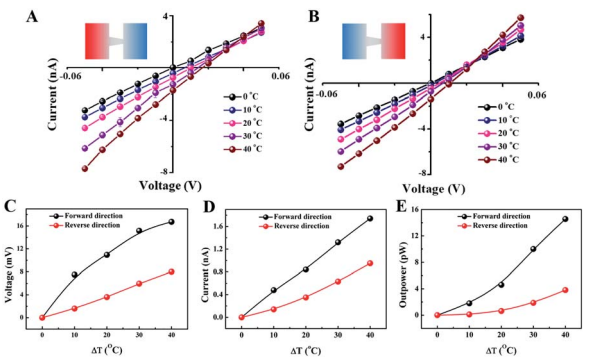

Fig. 3 Theoretical thermometric conversion capability. The base side was repositioned towards the cold side or hot side. (A) The *I–V* curves of the forward direction at different temperature differences and (B) those in the reverse direction. (C) Short-circuit current. (D) Open-circuit voltage. Both were obtained by the intercept of the abscissa and ordinate axes. (E) Outpower calculated by geometric area enclosed by the *I–V* curves and coordinate axes.

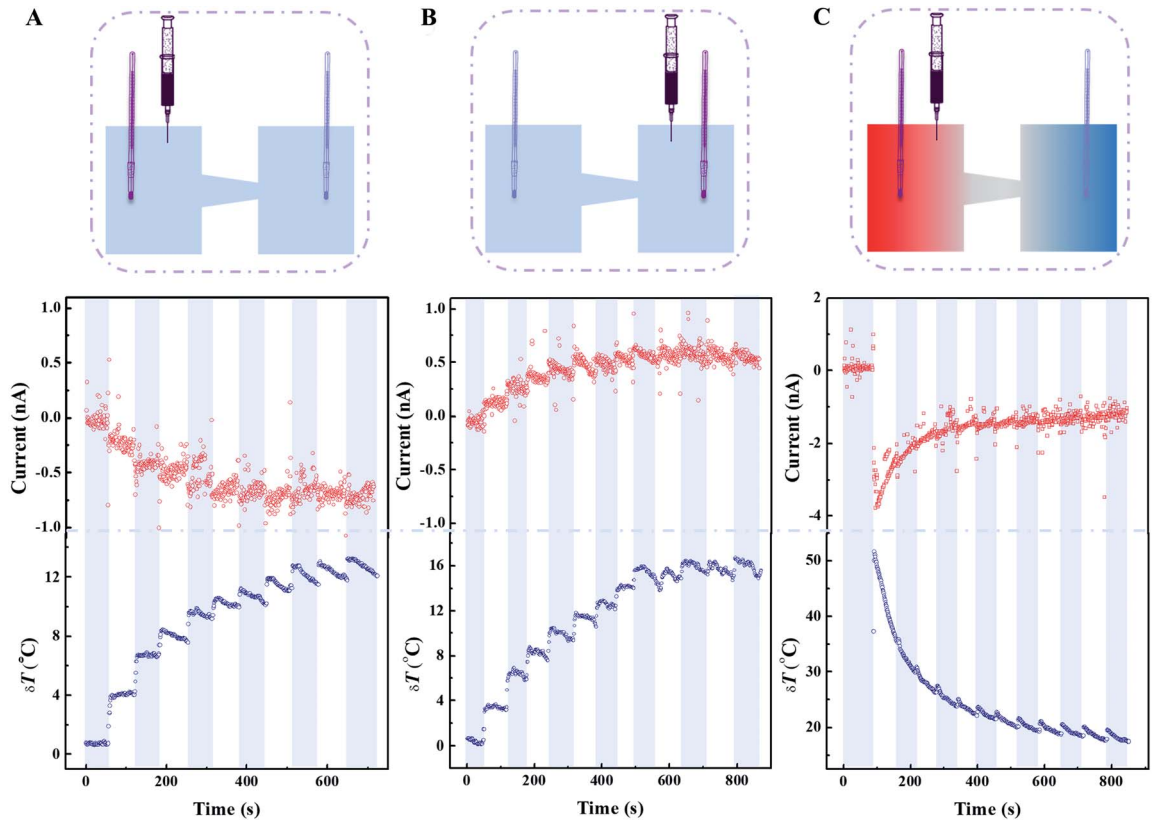

Fig. 4 Streaming current of a single nanochannel. The hot salty solution was added dropwise to a volume of 1 mL. (A) It was immersed into the cell of the base side and (B) it was immersed into the cell of the tip side. No temperature difference existed at the initial stage. (C) It was immersed into the cell of the base side to reduce the attenuation of temperature. No other equipment was employed except natural cooling. The current decreased regularly with the temperature difference.

time spans of 50–70 s (Fig. 4A). Prolonging the time span to 100–120 s, the system still possessed the excellent capability of thermoelectric conversion (Fig. S14†). Large intervals of time that result in the growth of the temperature difference at the next operation cause an obvious current oscillation. (2) All else being equal, only change the direction of feeding of the hot electrolyte (Fig. 4B). Under the same temperature gradient, the capability to convert temperature into electric signals decreased slightly, but the sensitivity of responding to the temperature variation was superior to that of the previous items. The principal reason is that the electrostatic interaction between the ions and pore wall impedes a positive ion motion from the base to the tip side. (3) The nanodevice generated an impressive streaming current under a larger temperature gradient (Fig. 4C). A momentary rise of temperature gradient would benefit power generation, indicating that a considerable power output can be maintained by the existence of a constant temperature gradient. Interestingly, a tiny temperature gradient would result in visible current oscillations even and multiple temperature changes show the fascinating sensitivity of temperature. Overall, the streaming current was fostered by an ongoing temperature gradient and possessed excellent sensitivity for temperature variation depending on time interval. The nanodevice could generate a steady and efficient electric power at normal operating conditions and has promising potential in the on-line temperature detection of nanofluids. When met improper operation, such as sudden decline of temperature gradient or abnormal reverse-direction temperature gradient, the nanodevice still has the capability to monitor sensitively the faults while maintaining power output to some extent.

Counter-pressure mass transport

Another exciting phenomenon has shown promise for directed ion transport under an adverse pressure gradient. The continuous addition of hot electrolyte carries a beneficial thermal energy as well as destroying the pressure equilibrium, but the final current depends on thermal energy (temperature gradient) rather than potential energy (pressure difference). To be clear, the nanodevice has been developed into a prototype with the function of transmembrane ion transport under an adverse pressure gradient. In a single nanochannel, the external pressure that reinforces the liquid flow is too gigantic to exceed the mechanical stress that materials could bear (Section S16†). In other words, small quantities of pressure difference have a negligible effect on liquid dynamics for a single nanochannel. As a consequence, we adopted a porous PI membrane as an ion motor to exemplify the advantage of an adverse pressure gradient. The effect of the pressure parameter was investigated, excluding temperature factors for five cycles (Fig. 5A). The

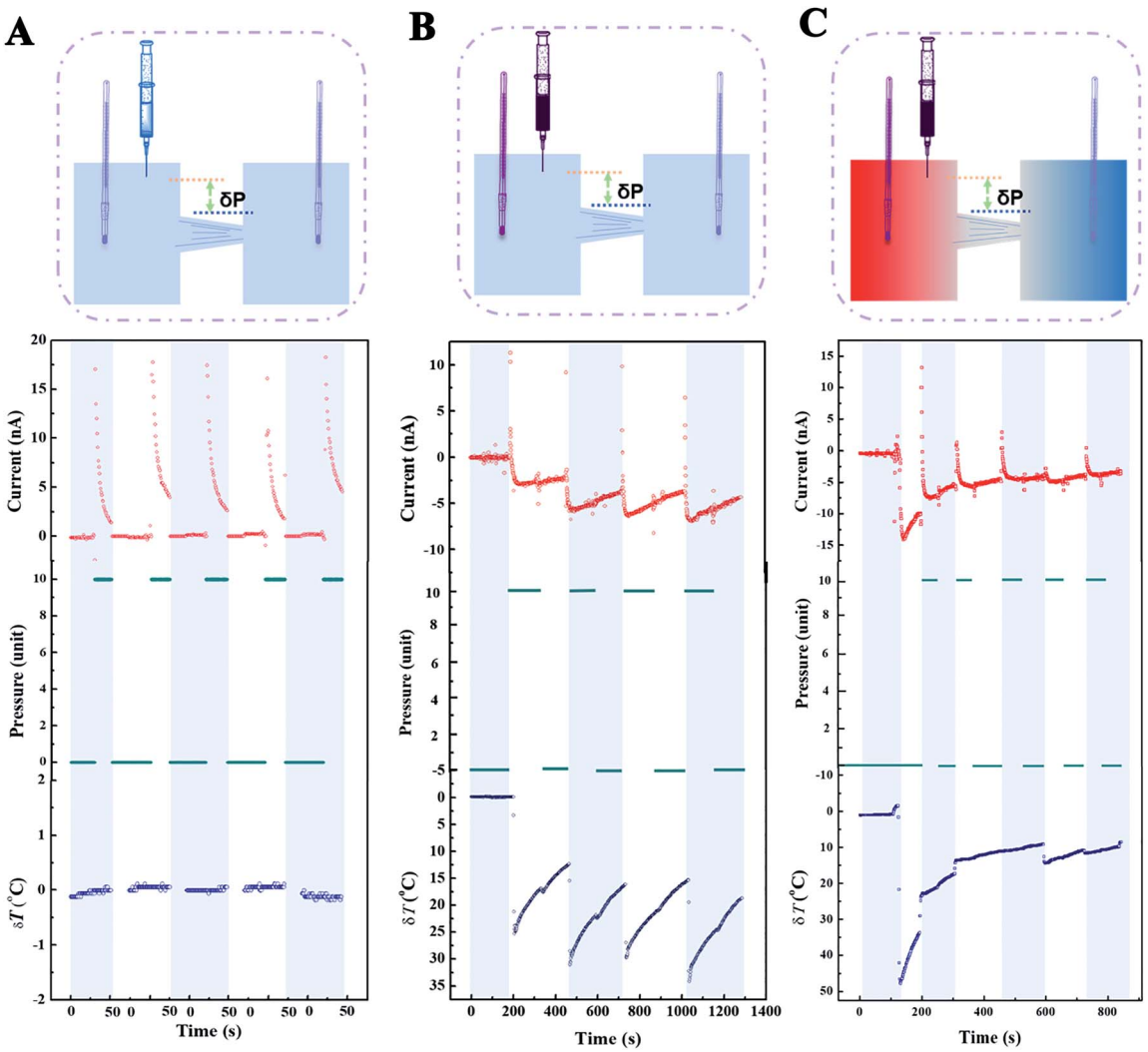

Fig. 5 Streaming current of porous membrane (10^6 cm^{-2}). (A) Streaming current induced by a pressure difference (500 Pa). The average current was estimated at about 17 nA using five experimental results. (B) Streaming current generated by temperature difference to support against the effect of pressure. The hot electrolyte was stepwise dropped into the system to enhance the temperature difference. The current changed from positive to negative indicating the rate of pressure and temperature were different. (C) Streaming current generated by a huge temperature difference. It reduced sharply due to the decrease of temperature difference.

averaged maximal streaming current (~17 nA) could be obtained by a pressure difference of $\delta P = 500$ Pa. Afterwards, the nanofluid was regulated by pressure and temperature in the process where the hot electrolyte was immersed into the system (Fig. 5B). The current changed from positive to negative immediately when the hot sources were immersed, which implied the transmitted speed of pressure was faster than that of temperature. And the influence of the temperature gradient outplayed its rival in the contest in the short term (Fig. S15†). Multiple deliberate operations were acted until the temperature difference changed intermittently. It was observed that an increase in the negative current resulted from the ascent of temperature gradient (Fig. S16†). Because the dissipation speed of heat depends on the volume of the bulk phase, the ratio of the current varied before and after removing the external pressure in each process. To examine the ability of ion transport, the nanodevice was tested under the regulation of temperature and pressure (Fig. 5C). Note that a streaming current of 14 nA at a temperature gradient of 47.5 °C was attained at the beginning. The variation in current approached an asymptotic value *via* reiterative modulation of the pressure and temperature gradient. Ultimately, 3 nA was obtained at a temperature gradient of 7 °C under a confrontational pressure gradient (Fig. S17†).

3. Conclusion

In summary, a novel nanodevice has been developed to realize the delicate multifunction of ion transport and power generation by harvesting low-grade heat. The streaming current can be modulated as expected by pH stimuli, mechanisms illuminated convincingly based on the coordination of theoretical computation and experimental results. The nanodevice is not only a conventional facility in energy conversion, separation and

water desalination but could also possibly apply to complex logic circuits and digital signal processing.

Conflicts of interest

There are no conflicts to declare.

Acknowledgements

This work was supported by the National Key R&D Program of China (2017YFA0206904, 2017YFA0206900), the National Natural Science Foundation of China (21625303, 51673206, 21434003, 21905287), the Strategic Priority Research Program of the Chinese Academy of Sciences (XDA2010213), Beijing Natural Science Foundation (2194088), Beijing Municipal Science & Technology Commission No. Z181100004418013, and the Key Research Program of the Chinese Academy of Sciences (QYZDY-SSW-SLH014).

References

1 M. Haras and T. Skotnicki, *Nano Energy*, 2018, **54**, 461.
2 S. Xia, X. Wu, Z. Zhang, Y. Cui and W. Liu, *Chem*, 2019, **5**, 753–785.
3 S. Chu, Y. Cui and N. Liu, *Nat. Mater.*, 2016, **16**, 16.
4 R. J. Holmes, *Science*, 2018, **360**, 854–855.
5 A. Siria, M.-L. Bocquet and L. Bocquet, *Nat. Rev. Chem.*, 2017, **1**, 0091.
6 S. Maniarasu, V. Manjunath, G. Veerappan and E. Ramasamy, in *Flexible Perovskite Solar Cells*, 2018, pp. 341–371.
7 Z. Zhang, X. Li, J. Yin, Y. Xu, W. Fei, M. Xue, Q. Wang, J. Zhou and W. Guo, *Nat. Nanotechnol.*, 2018, **13**, 1109–1119.
8 L. Li and Q. Wang, *Small*, 2018, 1800369.
9 L. Fu, S. Merabia and L. Joly, *J. Phys. Chem. Lett.*, 2018, **9**, 2086–2092.
10 J. Han and H. G. Craighead, *Science*, 2000, **288**, 1026–1029.
11 H. Lotien Richard, E. C. Cox, R. H. Austin and J. C. Sturm, *Science*, 2004, **304**, 987–990.
12 A. Würger, *Phys. Rev. Lett.*, 2008, **101**, 108302.
13 A. M. Benneker, H. D. Wendt, R. G. Lammertink and J. A. Wood, *Phys. Chem. Chem. Phys.*, 2017, **19**, 28232–28238.
14 R. Li, X. Fan, Z. Liu and J. Zhai, *Adv. Mater.*, 2017, **29**, 1702983.
15 K. Xiao, L. Wen and L. Jiang, *Small*, 2016, **12**, 2810–2831.
16 C. Liu and Z. G. Li, *Phys. Rev. Lett.*, 2010, **105**(17), 174501.
17 M. C Yang and M. Ripoll, *Soft Matter*, 2016, **12**, 8564–8573.
18 B. X. Xu, L. Liu, H. Lim, Y. Qiao and X. Chen, *Nano Energy*, 2012, **1**(6), 805–811.
19 C. Liu and Z. Li, *J. Chem. Phys.*, 2010, **132**, 024507.
20 M. Dietzel and S. Hardt, *Phys. Rev. Lett.*, 2015, **116**, 225901.
21 A. P. Straub, N. Y. Yip, S. Lin, J. Lee and M. Elimelech, *Nat. Energy*, 2016, **1**(7), 16090.
22 G. Xie, P. Li, Z. Zhang, K. Xiao, X. Y. Kong, L. Wen and L. Jiang, *Adv. Energy Mater.*, 2018, **8**, 1800459.
23 K. Chen, L. Yao and B. Su, Bionic Thermoelectric Response with Nanochannels, *J. Am. Chem. Soc.*, 2019, **141**(21), 8608–8615.
24 K. Xiao, X.-Y. Kong, Z. Zhang, G. Xie, L. Wen and L. Jiang, *J. Photochem. Photobiol., A*, 2016, **26**, 31–47.
25 C. Zhao, J. Lu, J. Hou, X. Y. Li, J. Wang, L. Jiang, H. T. Wang and H. C. Zhang, *Adv. Funct. Mater.*, 2018, **29**(6), 1806416.
26 E. A. Lumpkin and M. J. Caterina, *Nature*, 2007, **445**, 858–865.
27 V. Thomas, D. Guy, W. Ulrich, J. Annelies, F. Veit and N. Bernd, *Nature*, 2004, **430**, 748–754.
28 I. S. Ramsey, M. Delling and D. E. Clapham, *Annu. Rev. Physiol.*, 2006, **68**, 619–647.
29 L. Wen, X. Zhang, T. Ye and L. Jiang, *Sci. China Mater.*, 2018, 1–6.
30 X. Zhang, H. Liu and L. Jiang, *Adv. Mater.*, 2019, **31**, 1804508.
31 L. Chong and L. Zhigang, *Phys. Rev. Lett.*, 2010, **105**, 174501.
32 C. Liu and Z. Li, *J. Chem. Phys.*, 2010, **132**, 024507.
33 C. Liu and Z. Li, *Phys. Rev. E: Stat., Nonlinear, Soft Matter Phys.*, 2009, **80**, 036302.
34 H. A. Lee, Y. Ma, F. Zhou, S. Hong and H. Lee, *Acc. Chem. Res*, 2019, **52**(3), 704–713.
35 L. Haeshin, S. M. Dellatore, W. M. Miller and P. B. Messersmith, *Science*, 2007, **318**, 426–430.
36 Z. Zhang, X. Y. Kong, K. Xiao, G. Xie, Q. Liu, Y. Tian, H. Zhang, J. Ma, L. Wen and L. Jiang, *Adv. Mater.*, 2016, **28**, 144–150.
37 H. Zhang, X. Hou, Z. Yang, D. Yan, L. Li, Y. Tian, H. Wang and L. Jiang, *Small*, 2015, **11**, 786–791.
38 X. He, K. Zhang, T. Li, Y. Jiang, P. Yu and L. Mao, *J. Am. Chem. Soc.*, 2017, **139**, 1396–1399.
39 C.-Y. Lin, L.-H. Yeh and Z. S. Siwy, *J. Phys. Chem. Lett.*, 2018, **9**, 393–398.
40 X. He, K. Zhang, Y. Liu, F. Wu, P. Yu and L. Mao, *Angew. Chem., Int. Ed.*, 2018, **130**, 4680–4683.
41 Z. S. Siwy, *Adv. Funct. Mater.*, 2006, **16**, 735–746.
42 J. Koplik, J. R. Banavar and J. F. Willemsen, *Phys. Fluids A*, 1989, **1**, 781–794.
43 B. J. Kirby, *Micro-and nanoscale fluid mechanics: transport in microfluidic devices*, Cambridge university press, 2010.
44 K. Xiao, L. Chen, G. Xie, P. Li, X.-Y. Kong, L. Wen and L. Jiang, *Nanoscale*, 2018, **10**, 6850–6854.
45 A. P. Bregulla, A. Würger, K. Günther, M. Mertig and F. Cichos, *Phys. Rev. Lett.*, 2016, **116**, 188303.
46 L. Li and Q. Wang, *Small*, 2018, **14**, 1800369.

